Electronic Supplementary Information

Selective Adsorption of Trace Morpholine Impurities over *N*-Ethyl Morpholine by Tetralactam Solids

Shi-Yao Li,‡[a] Huan Yao,‡[a] Hao Hu,[a] Wen-Jie Chen,[a] Liu-Pan Yang,*[a,b] and Li-Li Wang*[a]

[a] *Hunan Province Cooperative Innovation Center for Molecular Target New Drug Study & School of Pharmaceutical Science, Hengyang Medical School, University of South China, Hengyang, Hunan, 421001, China. E-mail: yanglp@usc.edu.cn, wangll@usc.edu.cn.*

[b] *Department of Chemistry, Southern University of Science and Technology, Xueyuan Blvd 1088, Shenzhen, 518055, China.*

‡*These authors contributed equally to this work.*

Table of Contents

1. Experimental Section

1.1 General. All the reagents involved in this research were commercially available and used without further purification unless otherwise noted. Solvents were either employed as purchased or purified through standard laboratory procedures. ^{1}H, ^{13}C spectra were recorded on a Bruker Avance-500 NMR spectrometer. All chemical shifts were reported in ppm with residual solvents as the internal standards. The following abbreviations were used for signal multiplicities: s, singlet; d, doublet; dd, doublet of doublet; m, multiplet. Electrospray-ionization high-resolution mass spectrometry (ESI-HRMS) experiments were conducted on an applied Q EXACTIVE mass spectrometry system. Thin-layer chromatography (TLC) was carried out on 0.25 mm Yantai silica gel plates (60F-254). Column chromatography was performed using silica gel 60 (Tsingdao 40-63 nm, 300-400 mesh) as the stationary phase.

1.2 BET Surface Area Measurement. Brunauer-Emmett-Teller (BET) surface area measurement was performed on a Quantachrome Autosorb-iQ-C analyzer. Samples were degassed under dynamic vacuum for 12 h at 200 °C before each measurement. N_2 isotherms were measured using a liquid nitrogen bath (77 K)

1.3 Thermogravimetric Analysis. TGA analysis was carried out on a thermogravimertric analyzer (TGA2, METTLER TOLEDO, Switzerland). The samples were heated at a rate of 10 ℃ min^{-1}.

1.4 Powder X-ray Diffraction. Powder X-ray diffraction (PXRD) data were collected on a Rigaku Smartlab 9 kW X-ray diffractometer operating at 45 kV/200 mA using the Cu K_α line (λ = 1.5418 Å). PXRD patterns were measured over the 2θ range of 3−50° with 5° per min per step over 10 min.

1.5 Adsorption Experiments. In a typical solid-vapor sorption experiment, an open vial (5 mL) containing 20 mg of the activated solid of **1** was placed into a sealed vial (20 mL) containing 2 mL of morpholine (**MOR**), *N*-methyl morpholine (**NMM**) and *N*-ethyl morpholine (**NEM**) (single-component sorption), 1:1 mixture of **MOR** and

NEM (two-component sorption). And then activated adsorbent was heated at 30 °C for 30 min to remove any unbound **MOR**, **NMM** or **NEM** molecules adsorbed on the crystal surface after adsorption. The adsorption process was monitored over time by completely dissolving the solids in $CDCl_3$ and measuring the ratio of **MOR**, **NMM** and **NEM** to **1** by ^1H NMR experiments.

1.6 Gas Chromatography. Gas chromatography (GC) measurements were performed on an Agilent 7890B with an FID detector and a 2,3-diO-acetyl-6-0-TBDMS-β-cyclodextrin capillary column (Supelco Beta DEX 225; 30 mm × 0.25 mm × 0.25 μm). The following GC method was used: the oven was programmed from 50 °C, ramped at 2 °C/min increments to 100 °C with 15 min hold; injection temperature 250 °C; detection temperature 280 °C with nitrogen, air, and make-up flow-rates of 25, 400, and 30 mL/min, respectively; helium (carrier gas) flow-rate 2.0 mL/min.

1.7 DFT Calculation. Quantum chemistry calculations were performed by using Gaussian 09 package.[1] The structure of the complexes between host **1** and **NEM** has been optimized employing density functional theory (DFT) with dispersion corrected method (wB97XD)[2] in combination with 6-31G* basis set (the Polarizable Continuum Model (PCM) water model was used).[3]

1.8 solid-state NMR. Solid-state NMR measurements were performed on a Bruker Avance II 600 instrument operating at 600.2 and 150.9 MHz for ^1H and ^{13}C nuclei, respectively. Cylindrical 4 mm o.d. zirconia rotors with a sample volume of 80 μL were employed and spun at 10 kHz.

2. Synthetic Procedure

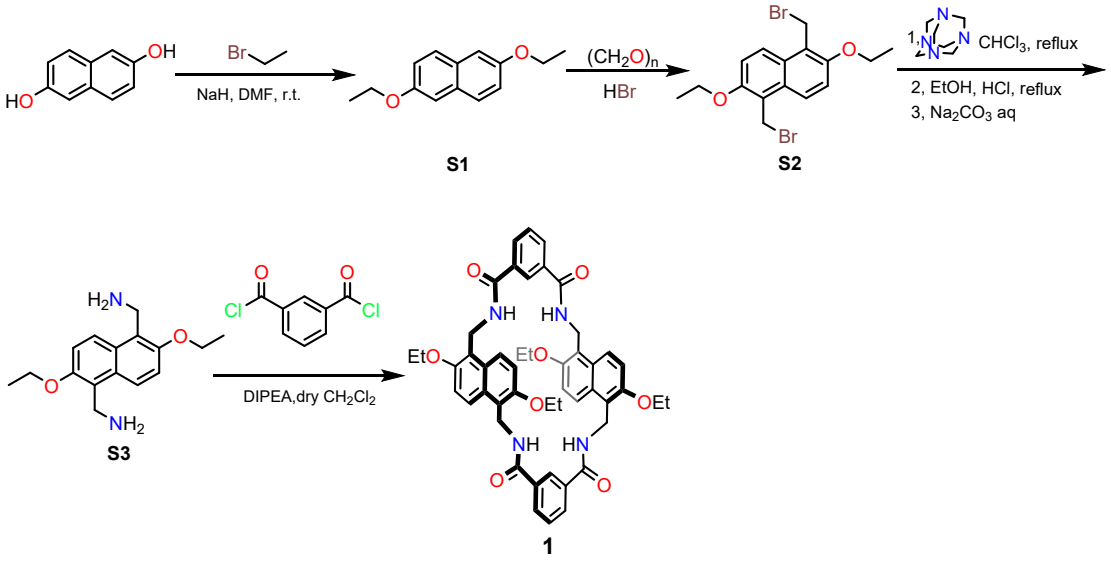

Compound **S1**, **S2** and **S3** were prepared followed a reported procedure.[4]

Macrocycle **1**: A solution of isophthaloyl chloride (0.89 g, 4.4 mmol) in anhydrous dichloromethane (50 mL) was added dropwise over 10 h (syringe pump) to a solution of **S3** (1.2 g, 4.4 mmol) and DIPEA (5 mL) in anhydrous dichloromethane (500 mL) under nitrogen. After stirring for a further 6 h, the solvent was removed under reduced pressure. The residue was dissolved in dichloromethane (100 mL) and washed with water (100 mL) and brine (100 mL). The organic solution was dried over Na_2SO_4 and evaporated in vacuo, then the solid was purified by column chromatography (CH_2Cl_2:MeOH = 100:1) to afford compound **1** as a white solid (534 mg, yield: 15%). ^{1}H NMR (500 MHz, $CDCl_3$, 298 K) δ [ppm] = 8.09 (d, J = 9.4 Hz, 4H), 8.08 (d, 4H), 7.57 (t, J = 7.9 Hz, 2H), 7.54 (s, 2H), 7.22 (d, J = 9.4 Hz, 4H), 6.35 (d, J = 6.2 Hz, 4H), 5.03 (s, 8H), 4.13 (q, J = 7.0 Hz, 8H), 1.41 (t, J = 7.0 Hz, 12H). ^{13}C NMR (126 MHz, Chloroform-d) δ [ppm] = 166.51, 153.41, 134.78, 129.27, 128.36, 125.32, 118.79, 115.30, 64.82, 34.94, 15.22. ESI-HRMS: m/z calcd for $[M+H]^+$ $C_{48}H_{48}N_4O_8^+$ 809.3545; found 809.3526 (error = 2.3 ppm).

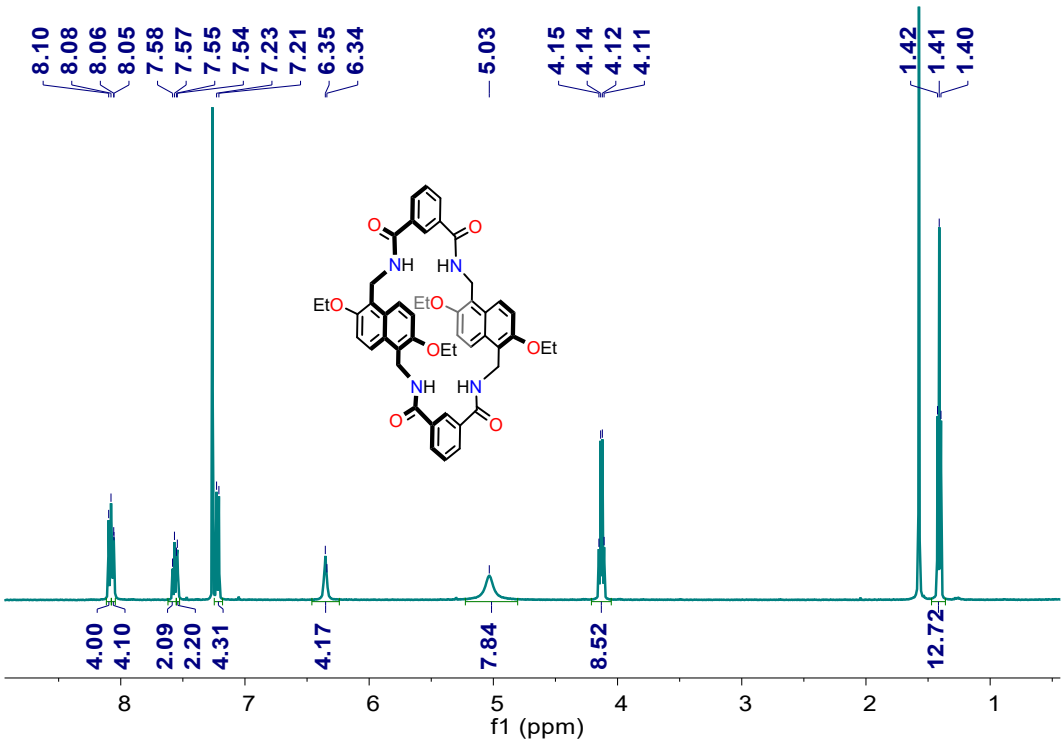

^{1}H NMR spectrum (500 MHz, $CDCl_3$, 298 K) of **1**

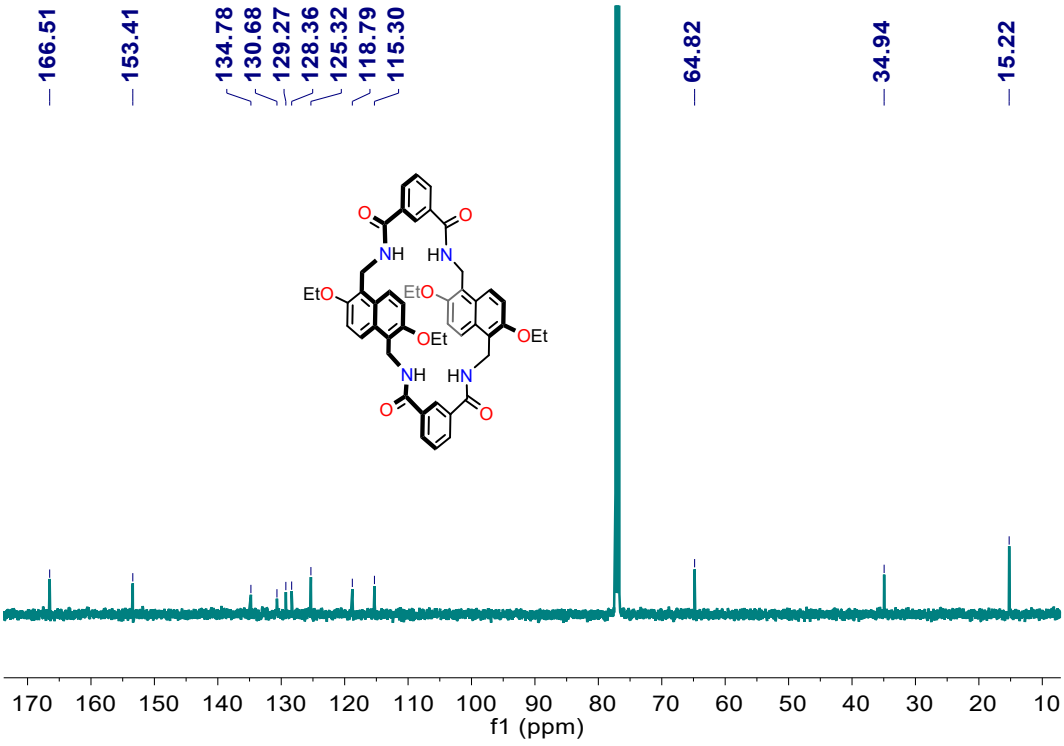

^{13}C NMR spectrum (126 MHz, $CDCl_3$, 298 K) of **1**

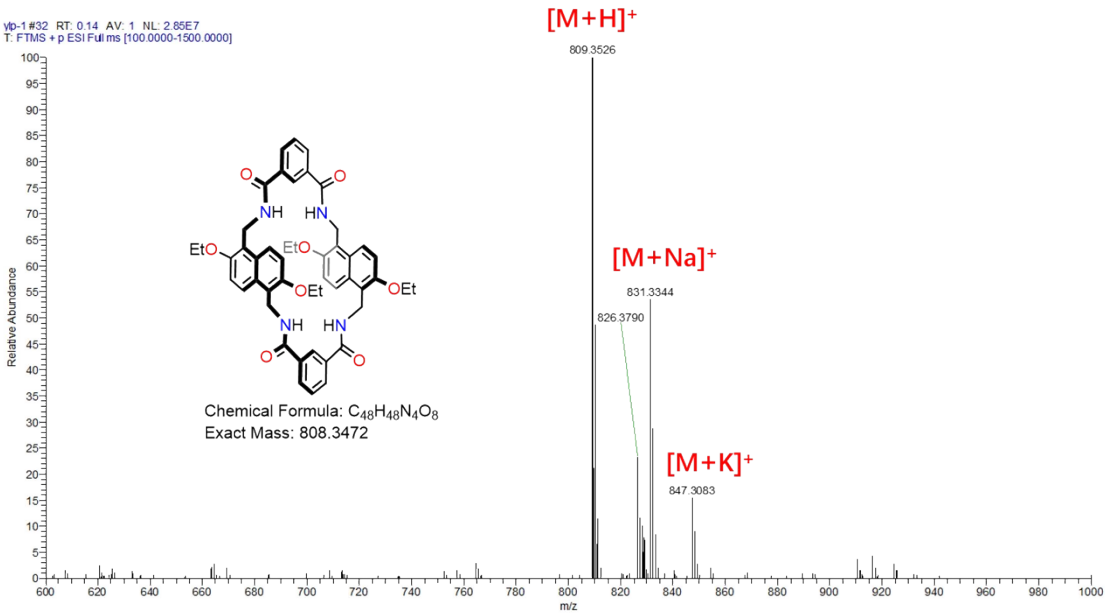

ESI mass spectrum of **1**

3. Characterization of Activated Crystals

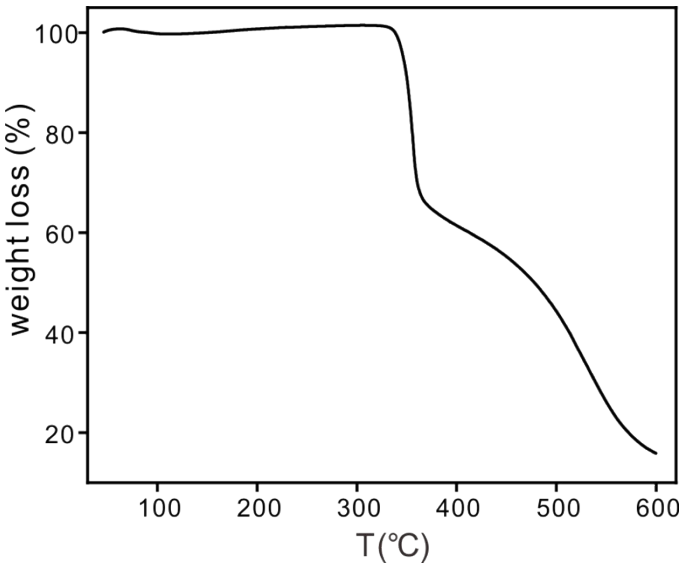

Fig. S1. TGA of the activated solid of **1**. Almost no weight loss occurs below 350 ℃, supporting that the residual solvents were completely removed through activation.

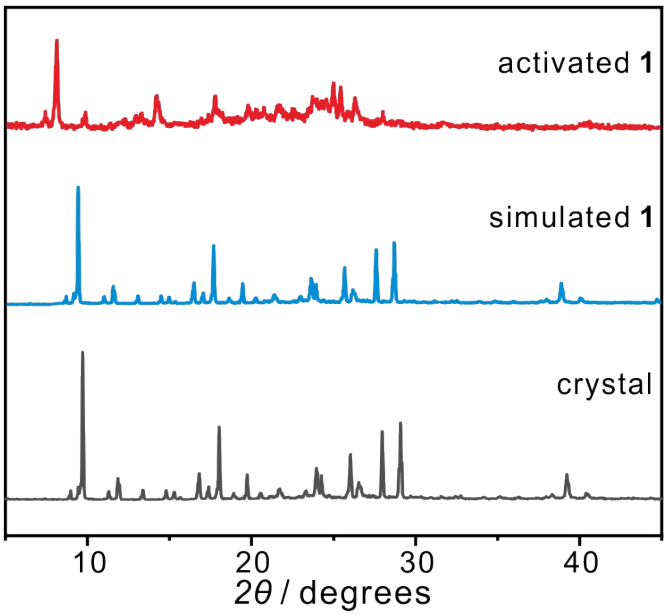

Fig. S2. Powder X-ray diffraction (PXRD) patterns of **1** before and after activation and the simulated PXRD pattern based on the crystal structure. The PXRD patterns show that the crystallinity was maintained after activation.

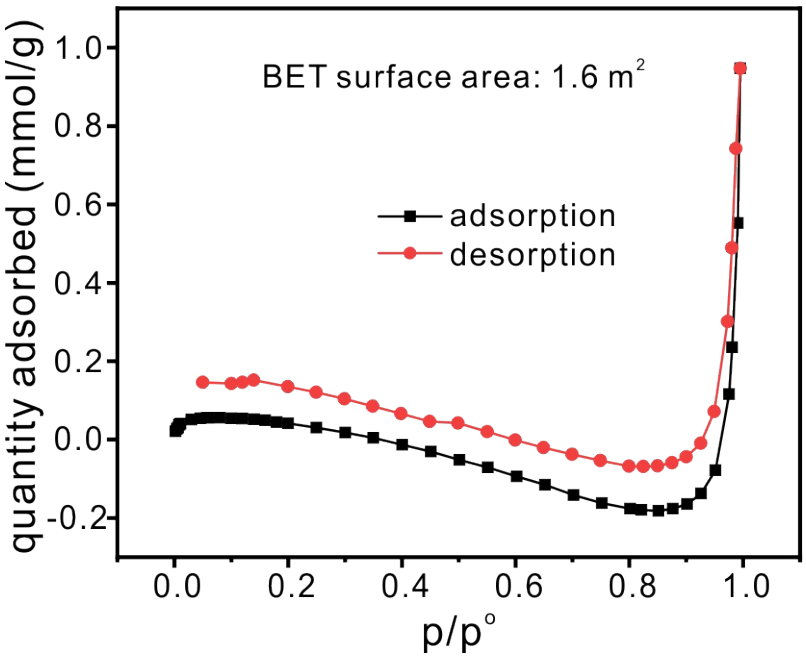

Fig. S3. N_2 adsorption isotherm of the activated solid of **1**. The BET surface area value is shown in the figure.

4. Solid–Vapor Adsorption Experiments

Table S1 Physical properties of the two components.

component	boiling point (°C)	melting point (°C)
MOR	129	-5
NEM	139	-83

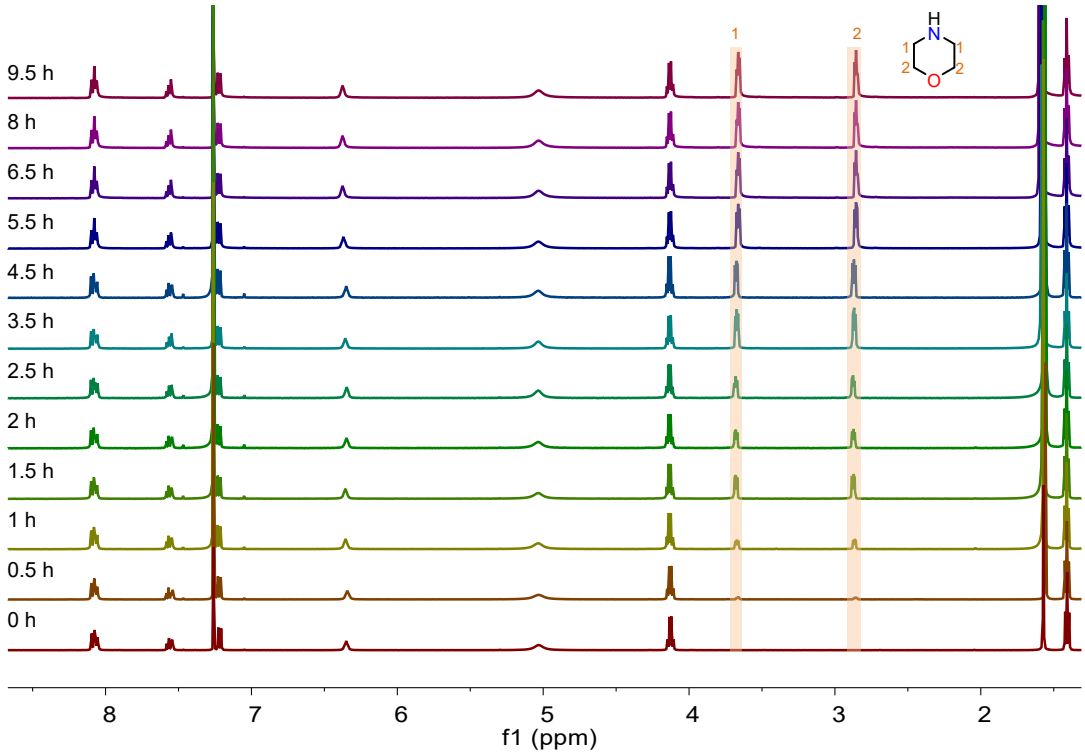

Fig. S4. Time-dependent ^{1}H NMR spectrum (500 MHz, $CDCl_3$, 298K) of **1** after adsorption of **MOR** vapor. From bottom to top, the spectra were recorded for 9.5 hours. The relative uptake of **MOR** by **1** is plotted in Fig. 3a.

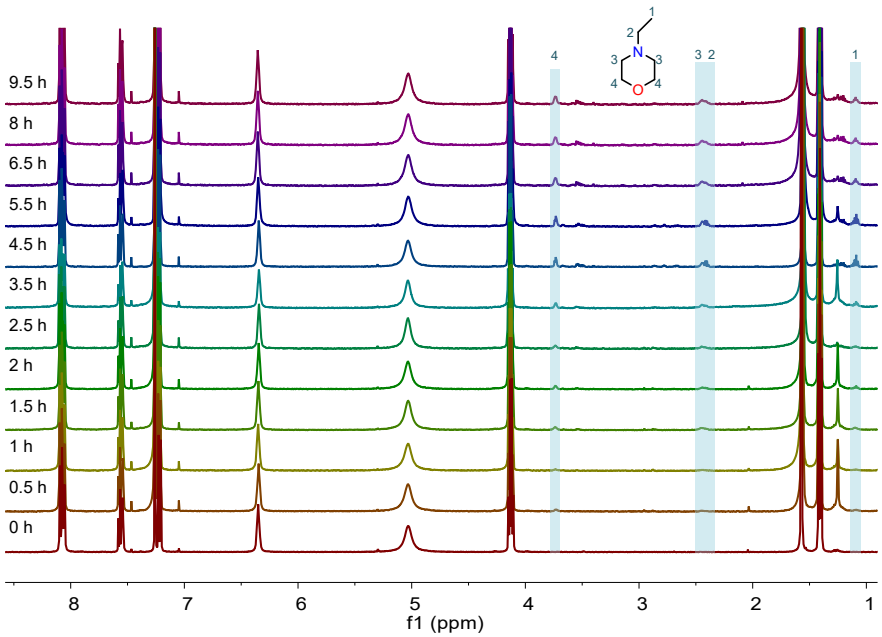

Fig. S5. Time-dependent ^{1}H NMR spectrum (500 MHz, $CDCl_3$, 298K) of **1** after adsorption of **NEM** vapor. From bottom to top, the spectra were recorded for 9.5 hours. The relative uptake of **NEM** by **1** is plotted in Fig 3a.

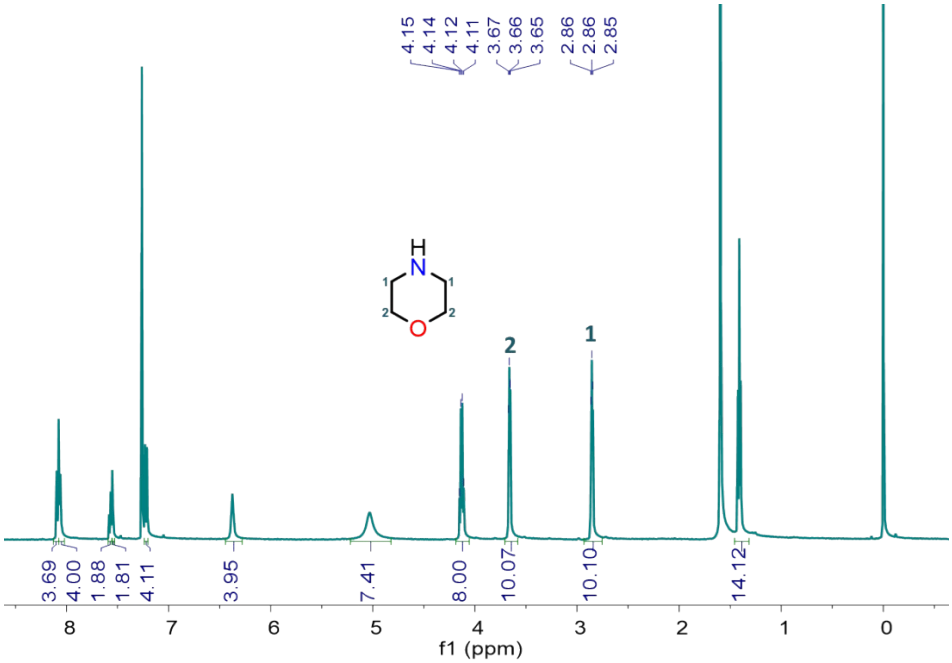

Fig. S6. ^{1}H NMR spectrum (500 MHz, 298K, $CDCl_3$) of **1** after being exposed to **MOR** for 9.5 h and heated at 30 °C for 30 min to remove the surface adsorption (HDO peak comes from trace amount of water in $CDCl_3$). Almost 2.5 eq. of **MOR** to **1** was adsorbed.

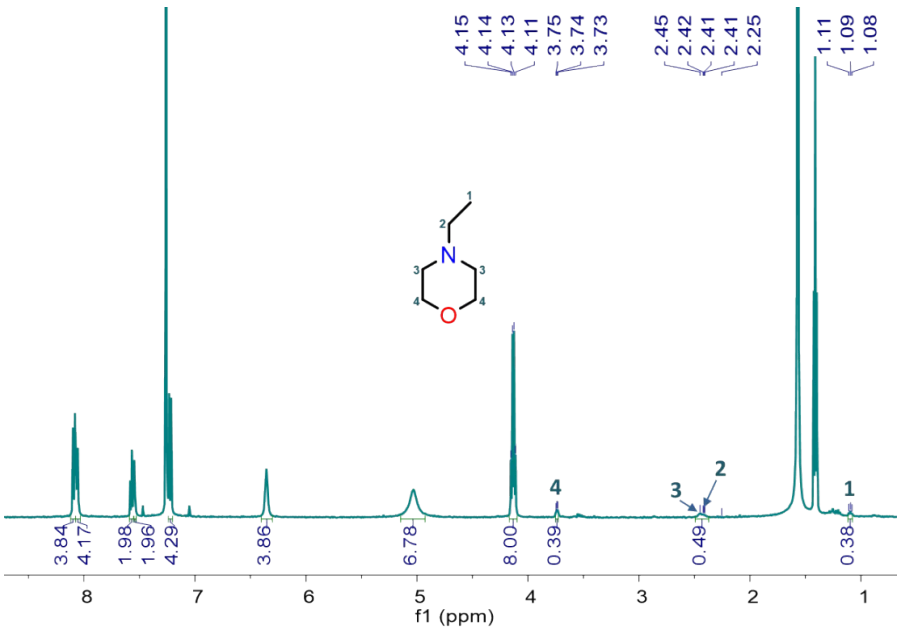

Fig. S7. ^{1}H NMR spectrum (500 MHz, 298K, $CDCl_3$) of **1** after being exposed to **NEM** for 9.5 h and heated at 30 °C for 30 min to remove the surface adsorption (HDO peak comes from trace amount of water in $CDCl_3$). Only about 0.2 eq. of **NEM** to **1** was adsorbed.

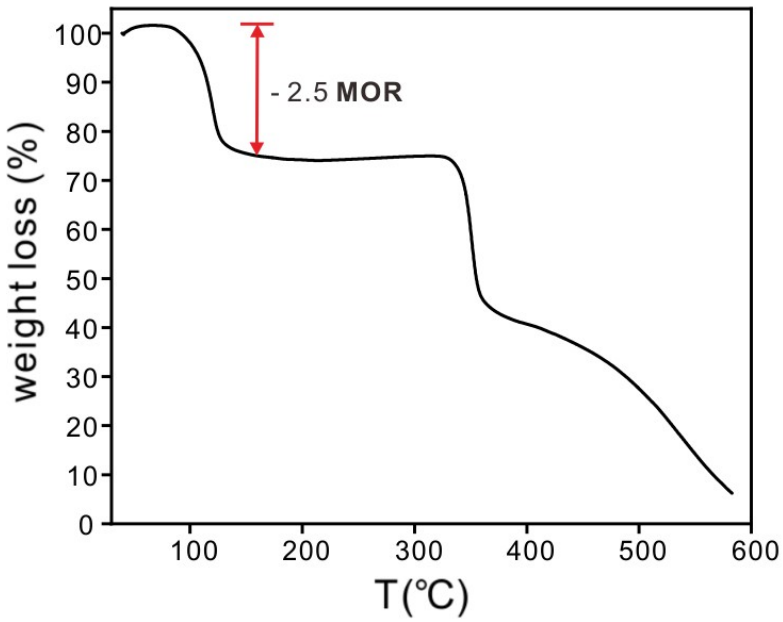

Fig. S8. TGA of the activated solid of **1** after adsorbing **MOR**. About 2.5 **MOR** molecules per host were lost at 130 °C.

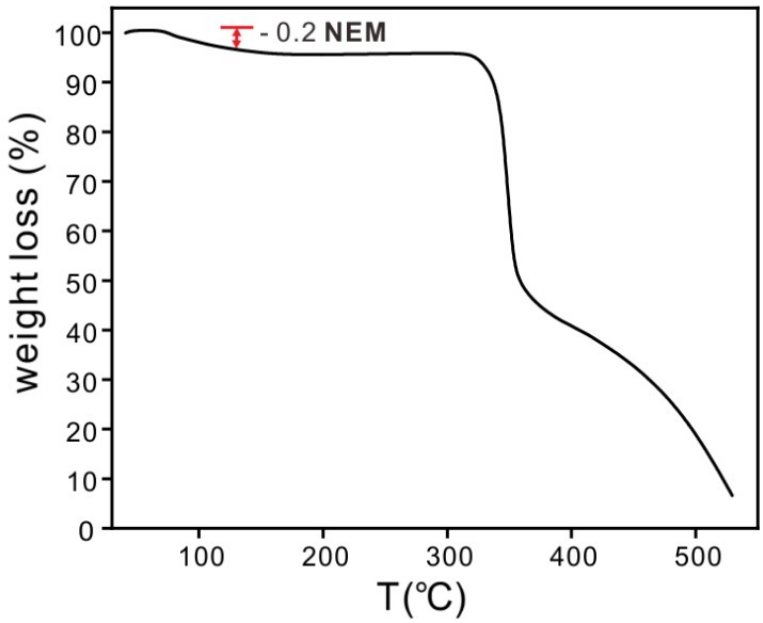

Fig. S9. TGA of the activated solid of **1** after adsorbing **NEM**. About 0.2 **NEM** molecules per host were lost at 120 ℃.

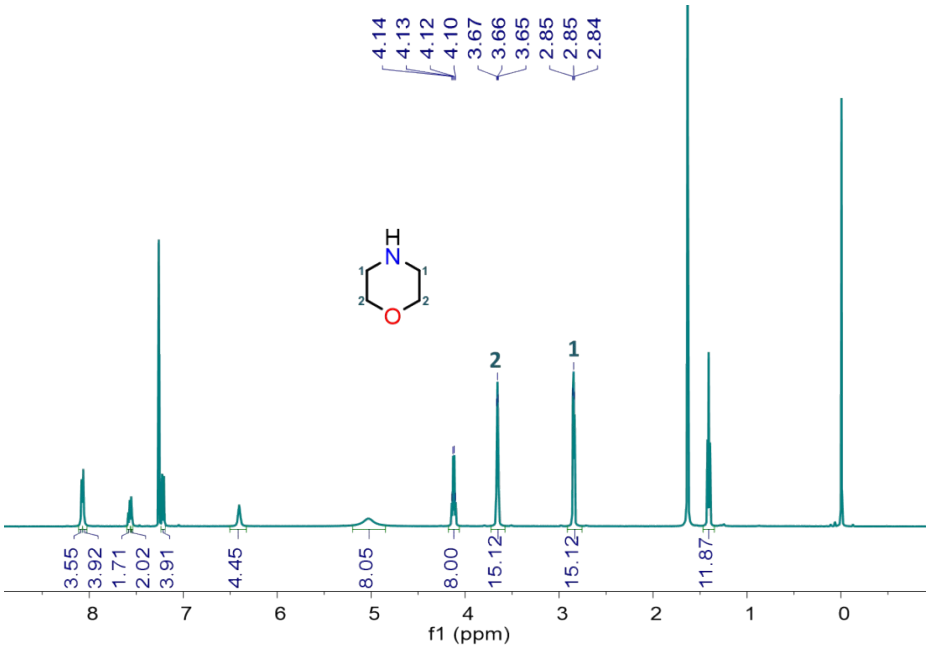

Fig. S10. ^{1}H NMR spectrum (500 MHz, 298K, $CDCl_3$) of **1** after being exposed to **MOR** for 12 h and not remove the surface adsorption (HDO peak comes from trace amount of water in $CDCl_3$). Almost 3.8 eq of **MOR** to **1** was adsorbed.

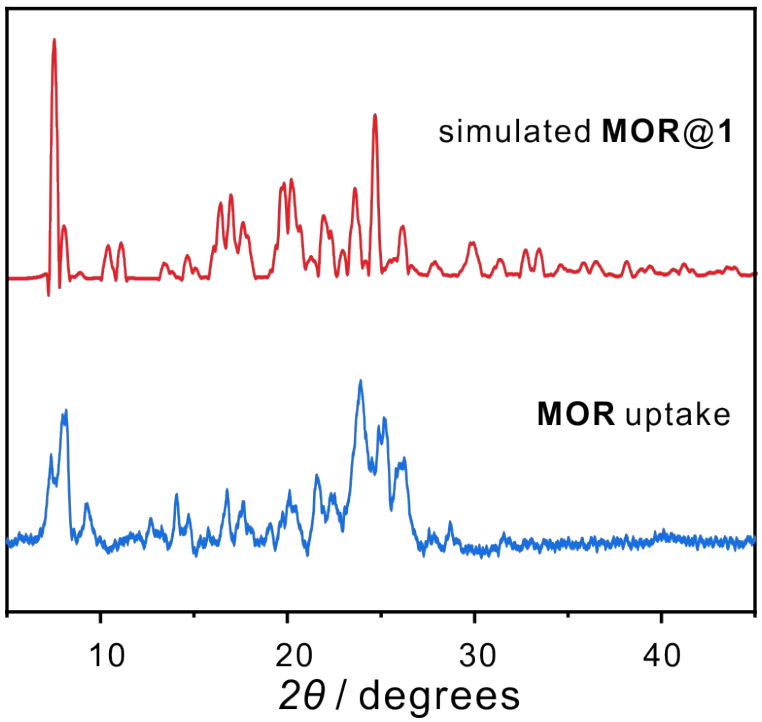

Fig. S11. Simulated PXRD pattern based on the crystal structure of **MOR@1** and PXRD pattern of activated **1** after adsorption of **MOR** vapor.

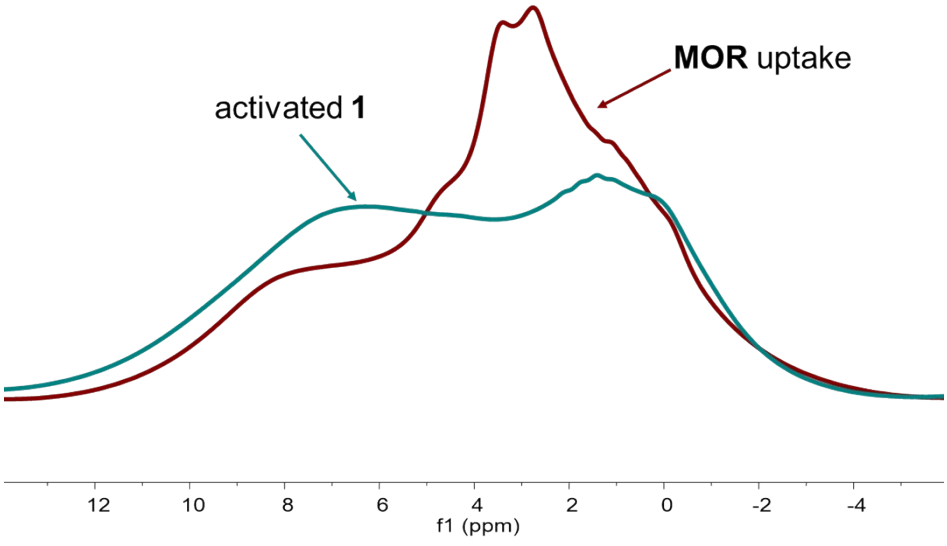

Fig. S12. ^{1}H solid-state NMR spectra of activated **1** and activated 1 following **MOR** uptake. The differences before and after absorbing **MOR** indicate structural changes in the adsorption process.

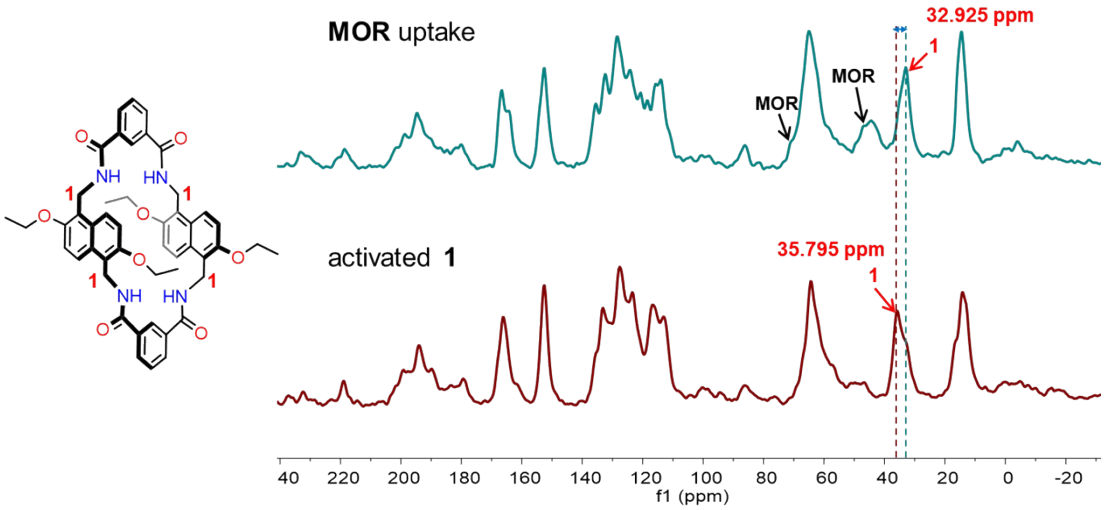

Fig. S13. ^{13}C solid-state NMR spectra of activated **1** and activated 1 following **MOR** uptake. The peaks around 44 ppm and 70 ppm can be assigned to **MOR**. The methylene carbon (35 ppm) in the bridge amide bond of the host undergoes an obvious shift following **MOR** uptake, supporting the formation of hydrogen bonding interactions between amide NH and **MOR**.

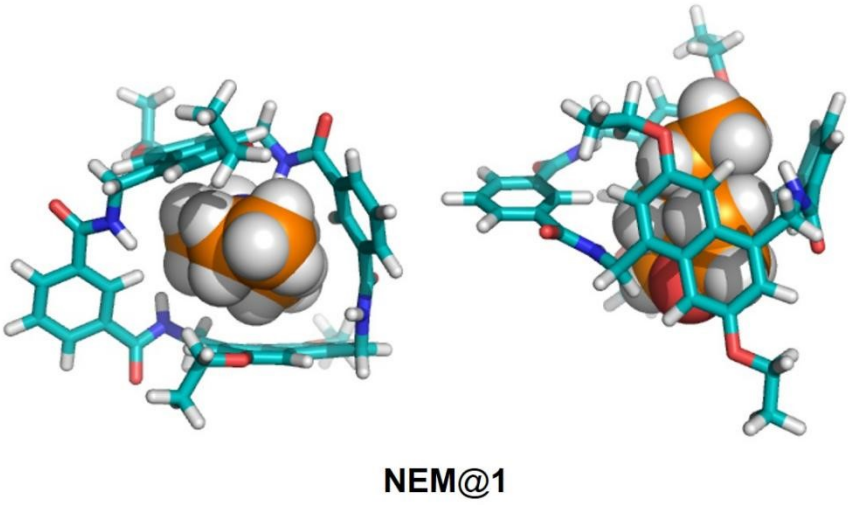

Fig. S14. Energy-minimized structures of complexes **NEM@1** calculated by DFT at the wB97XD/6-31G(d) level of theory.

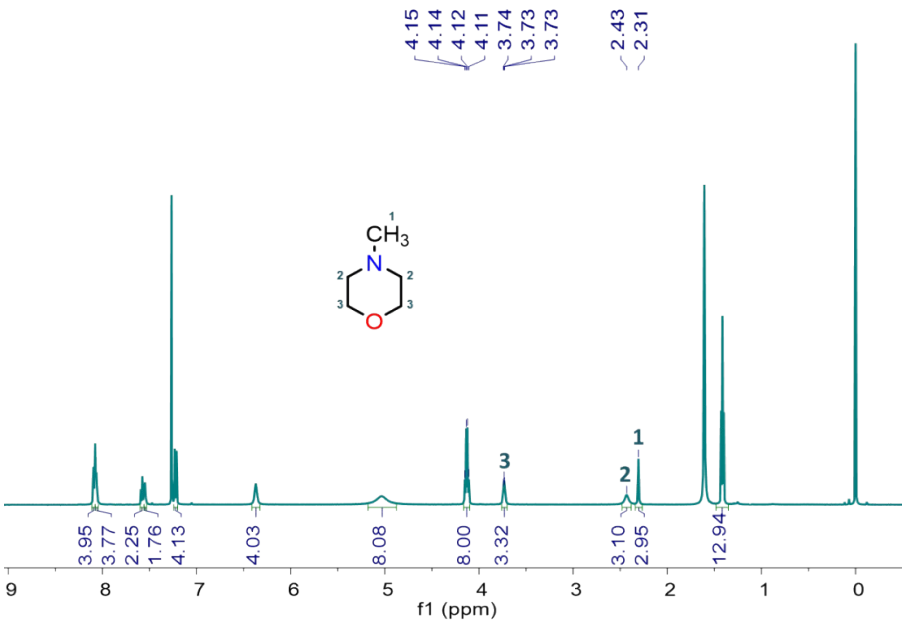

Fig. S15. ^{1}H NMR spectrum (500 MHz, 298K, $CDCl_3$) of **1** after being exposed to **NMM** for 9.5 h and heated at 30 °C for 30 min to remove surface adsorption (HDO peak comes from trace amount of water in $CDCl_3$). Almost 0.8 eq. of **NMM** to **1** was adsorbed.

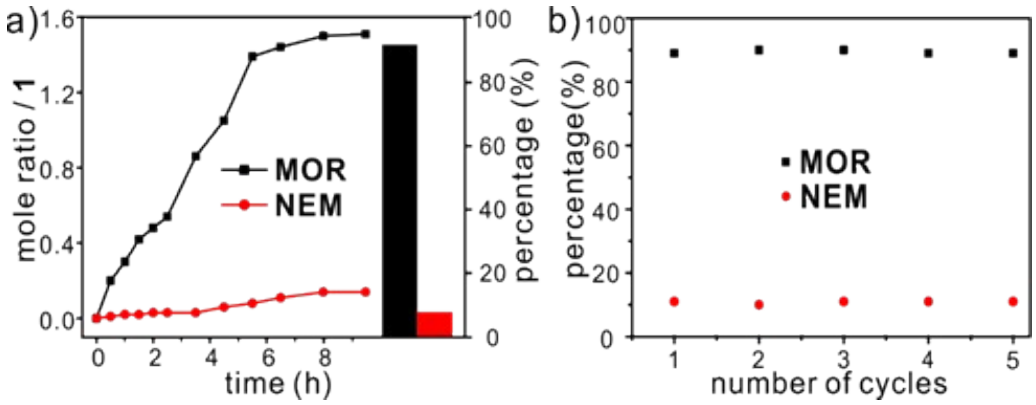

Fig. S16. a) Time-dependent two-component vapor-solid plots of **1** with 1:1 mixture of **MOR** and **NEM**, and the relative uptakes at 5.5 h; b) relative uptake ratios of **MOR** and **NEM** by **1** at 5.5 h after 5 recycles.

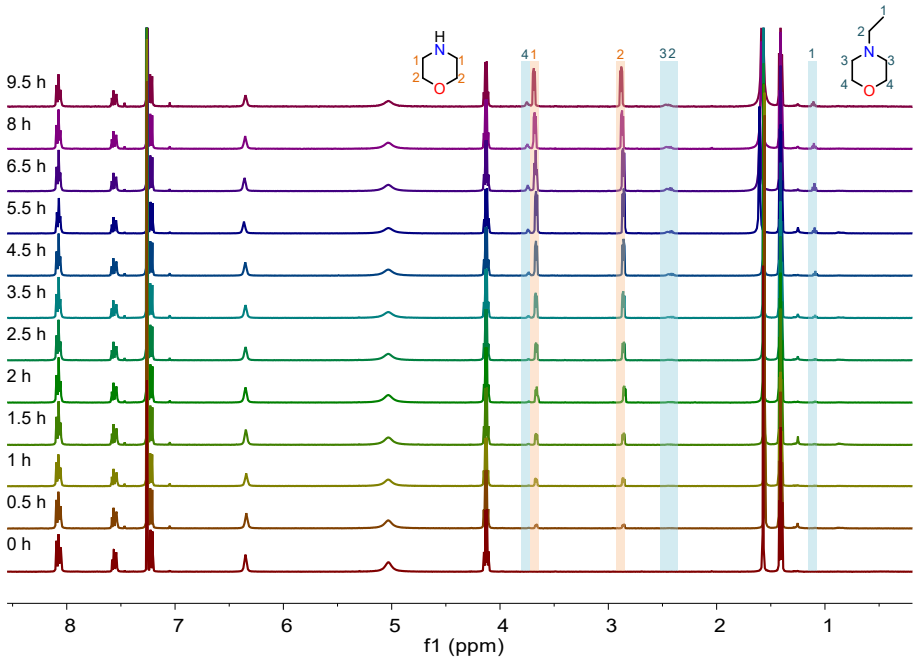

Fig. S17. Time-dependent ^{1}H NMR spectra ($CDCl_3$) of **1** after vapor adsorption of a mixture of **MOR** and **NEM**. From bottom to top, the spectra were recorded for 9.5 hours. The relative uptake of **MOR** and **NEM** by **1** is plotted in Fig. 5a.

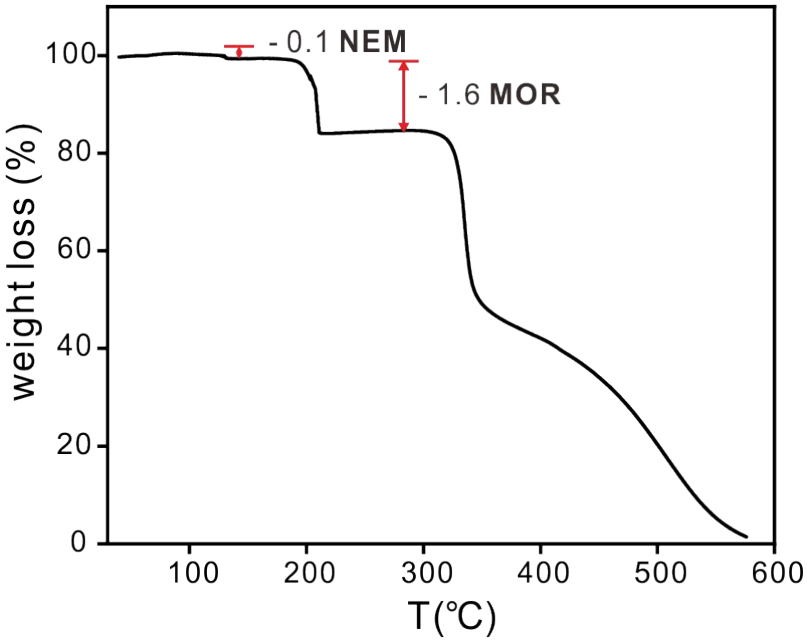

Fig. S18. TGA of the activated solid of **1** after vapor adsorption of mixture of **MOR** and **NEM**. About 0.1 **NEM** and 1.6 **MOR** molecules per host were lost at 130 °C and 180 °C.

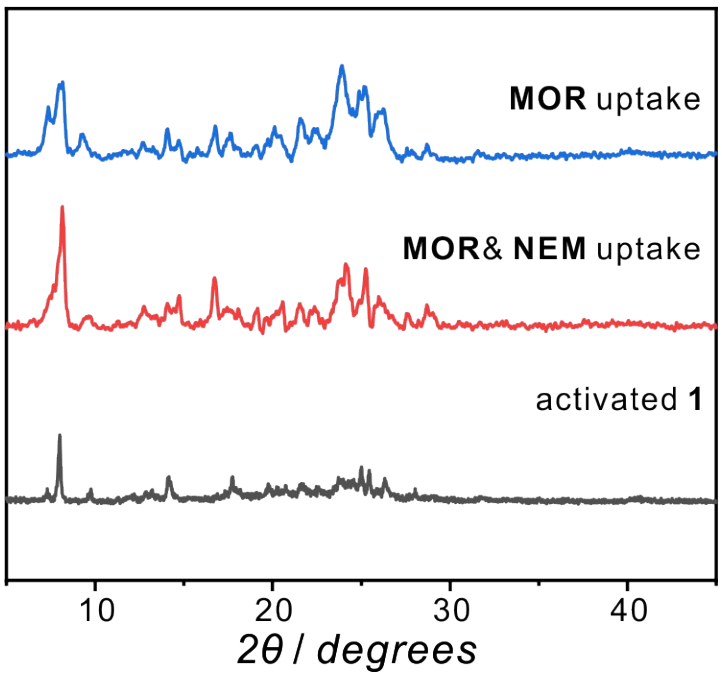

Fig. S19. PXRD pattern of activated **1**, activated **1** after adsorption of mixed **MOR** and **NEM** vapor, activated 1 after adsorption of **MOR** vapor.

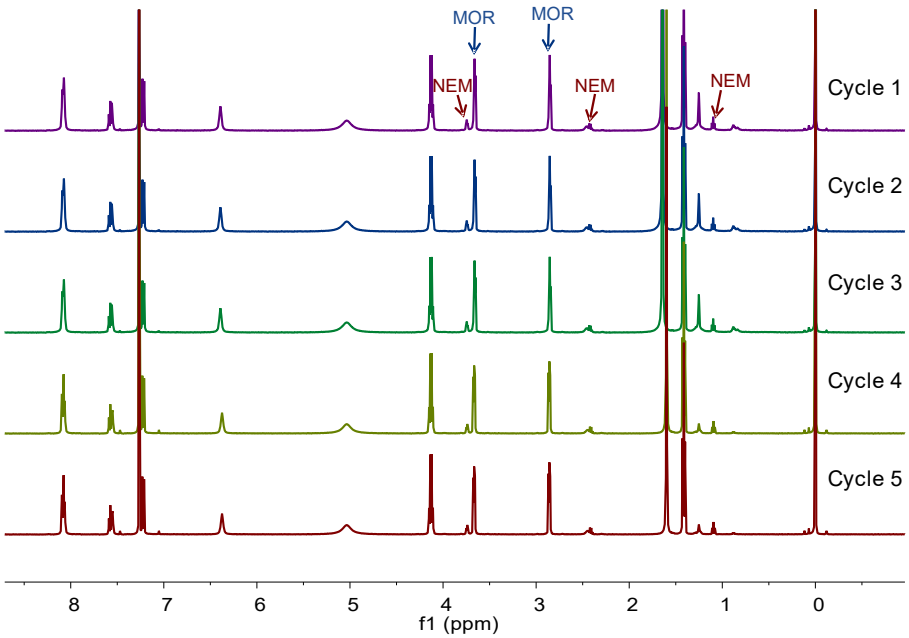

Fig. S20. ^{1}H NMR spectra (500 MHz, $CDCl_3$, 298 K) of solid-vapor adsorption repeatability experiments.

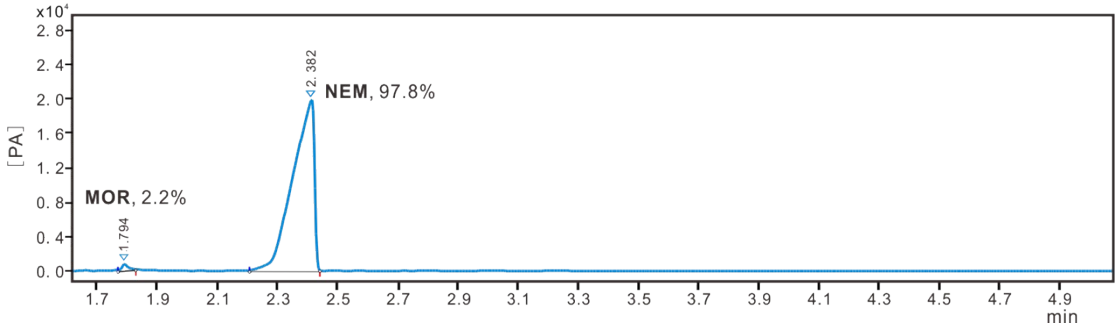

Fig. S21. The purity of **NEM** measured by GC before solid-vapor adsorption and solid-liquid adsorption.

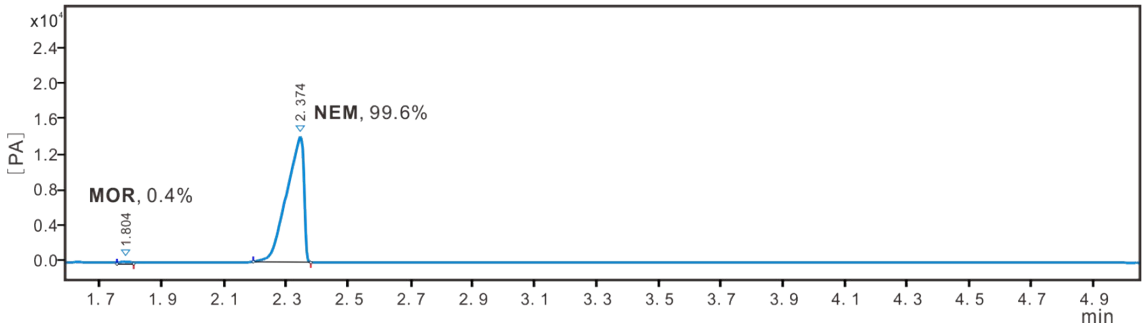

Fig. S22. The purity of **NEM** measured by GC after solid-vapor adsorption.

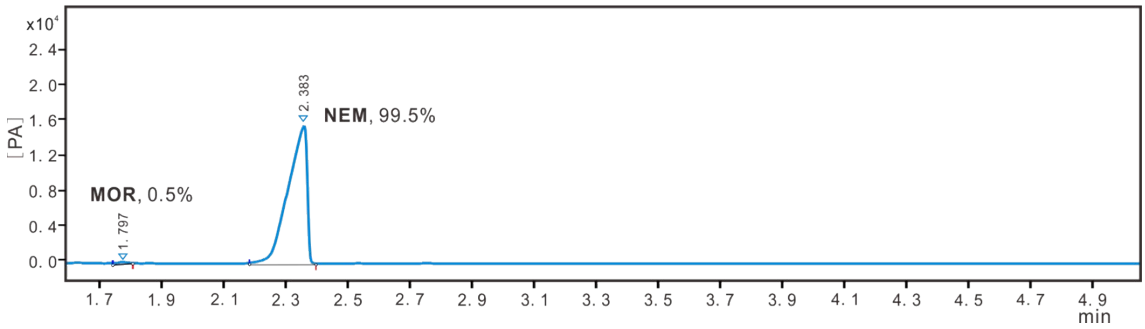

Fig. S23. The purity of **NEM** measured by GC after solid-liquid adsorption.

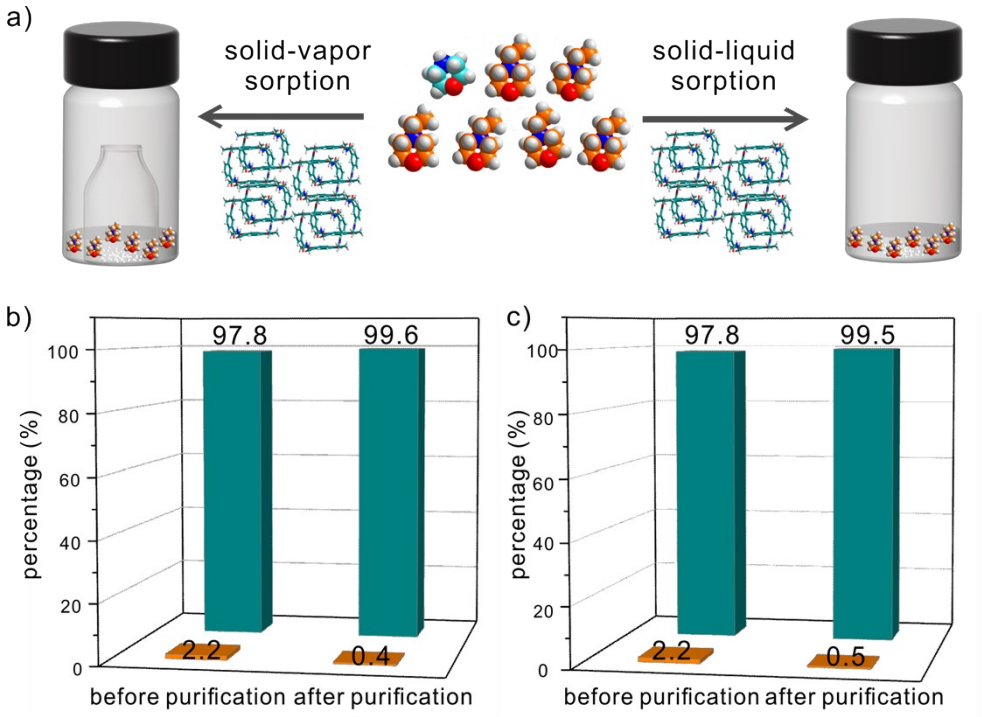

Fig. S24. a) Summary diagram of the purification of **NEM** by solid-vapor or solid-liquid sorption with **1**; The purity of 97.8% **NEM** before and after b) solid-vapor or c) solid-liquid sorption with **1**. The green and orange columns represent the percentage of **NEM** and **MOR**, respectively.

6. X-Ray Single Crystallography

Crystal data for was collected on a Bruker D8 VENTURE with Cu K_α radiation (λ = 1.54178 Å) at 173(2) K. The structures were solved by the direct method and different Fourier syntheses. All calculations were performed by full-matrix least-squares methods on F^2 by using the SHELX-97 program[5,6], all non-hydrogen atoms were refined with anisotropic thermal parameters and the hydrogen atoms were fixed at calculated positions and refined by a riding mode. SQUEEZE routine implemented on PLATON was used to remove electron densities corresponding to disordered solvent molecules in Crystal data.

Crystal data for **1:** $C_{50}H_{60}N_4O_{12}$, M = 945.05, triclinic, a = 9.483(2) Å b = 10.987(3) Å c = 12.790(3) Å, α = 68.707(7)°, β = 82.307(7)°, γ = 73.621(7)°, V = 1190.5(5) Å^3, T = 214.56 K, space group P-1, Z = 1, 18603 reflections measured, 4061 independent reflections (R_{int} = 0.0688, R_{sigma} = 0.0728). The final R_1 value was 0.0566 ($I > 2\sigma(I)$). The final $wR(F^2)$ value was 0.1328 ($I > 2\sigma(I)$). The final R_1 value was 0.0895 (all data). The final $wR(F^2)$ value was 0.1482 (all data). The goodness of fit on F^2 was 1.068. CCDC-2246207 contains the supplementary data for this structure. These data can be obtained free of charge via www.ccdc.cam.ac.uk/data_request/cif, or by emailing data_request@ccdc.cam.ac.uk, or by contacting The Cambridge Crystallographic Data Centre, 12, Union Road, Cambridge CB2 1EZ, UK; fax: +44 1223 336033.

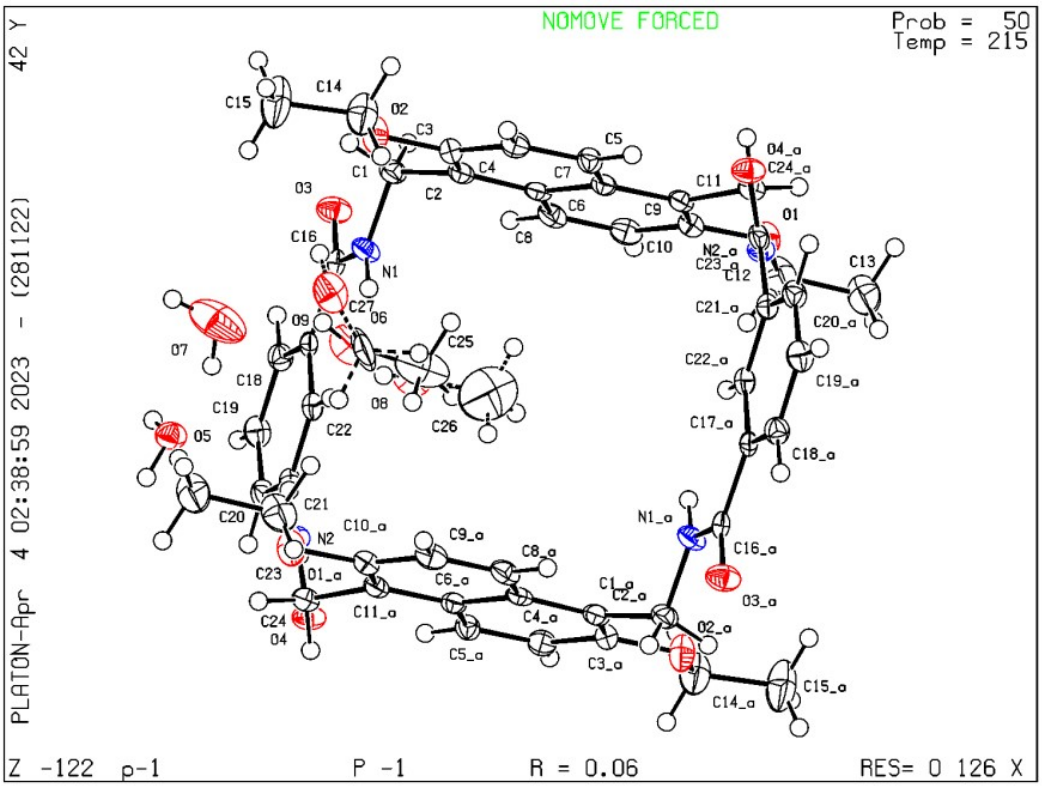

Crystal data for **MOR@1:** $C_{64}H_{84}N_8O_{12}$, M = 1157.39, triclinic, a = 11.4061(7) Å b = 11.5234(8) Å c = 13.0536(9) Å, α = 84.464(3)°, β = 65.455(3)°, γ = 74.125(3)°, V = 1500.87(18) Å^3, T = 100.0 K, space group P-1, Z = 1, 27092 reflections measured, 5325 independent reflections (R_{int} = 0.0607, R_{sigma} = 0.0596). The final R_1 value was 0.0533 ($I > 2\sigma(I)$). The final $wR(F^2)$ value was 0.1416 ($I > 2\sigma(I)$). The final R_1 value was 0.0894 (all data). The final $wR(F^2)$ value was 0.1566 (all data). The goodness of fit on F^2 was 1.096. CCDC-2246208 contains the supplementary data for this structure. These data can be obtained free of charge via www.ccdc.cam.ac.uk/data_request/cif, or by emailing data_request@ccdc.cam.ac.uk, or by contacting The Cambridge Crystallographic Data Centre, 12, Union Road, Cambridge CB2 1EZ, UK; fax: +44 1223 336033.

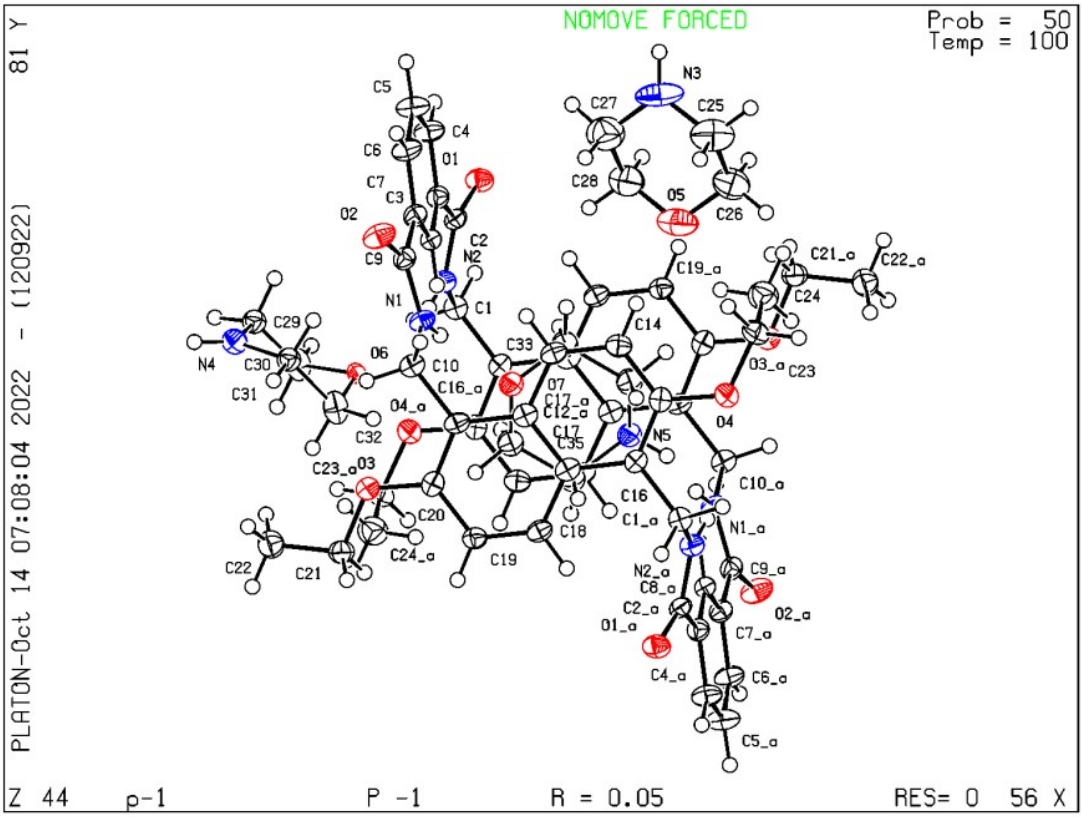

6. References

1. Frisch, M. J.; Trucks, G. W.; Schlegel, H. B.; Scuseria, G. E.; Robb, M. A.; Cheeseman, J. R.; Scalmani, G.; Barone, V.; Mennucci, B.; Petersson, G. A.; Nakatsuji, H.; Li, M.; Caricato, X.; Hratchian, H. P.; Izmaylov, A. F.; Bloino, J.; Zheng, G.; Sonnenberg, J. L.; Hada, M.; Ehara, M.; Toyota, K.; Fukuda, R.; Hasegawa, J.; Ishida, M.; Nakajima, T.; Honda, Y.; Kitao, O.; Nakai, H.;. Vreven, T.; Montgomery Jr., J. A.; Peralta, J. E.; Ogliaro, F.; Bearpark, M. J.; Heyd, J.; Brothers, E. N.; Kudin, K. N.; Staroverov, V. N.; Kobayashi, R.; Normand, J.; Raghavachari, K.; Rendell, A. P.; Burant, J. C.; Iyengar, S. S.; Tomasi, J.; Cossi, M.; Rega, N.; Millam, N. J.; Klene, M.; Knox, J. E.; Cross, J. B.; Bakken, V.; Adamo, C.; Jaramillo, J.; Gomperts, R.; Stratmann, R. E.; Yazyev, O.; Austin, A. J.; Cammi, R.; Pomelli, C.; Ochterski, J. W.; Martin, R. L.; Morokuma, K.; Zakrzewski, V. G.; Voth, G. A.; Salvador, P.; Dannenberg, J. J.; Dapprich, S.; Daniels, A. D.; Farkas, Ö.; Foresman, J. B.; Ortiz, J. V.; Cioslowski, J.; Fox, D. J. *Gaussian 09*, Gaussian, Inc.: Wallingford, CT, USA, **2013**.
2. Chai, J.-D.; Head-Gordon, M. Long-Range Corrected Hybrid Density Functionals with Damped Atom–Atom Dispersion Corrections. *Phys. Chem. Chem. Phys.,* **2008**, *10*, 6615-6620.
3. (a) Cances, E.; Mennucci, B.; Tomasi, J. A New Integral Equation Formalism for the Polarizable Continuum Model: Theoretical Background and Applications to Isotropic and Anisotropic Dielectrics. *J. Chem. Phys.,* **1997**, *107*, 3032; (b) Mennucci, B.; Tomasi, J. Continuum Solvation Models: A New Approach to the Problem of Solute's Charge Distribution and Cavity Boundaries. *J. Chem. Phys.,* **1997,** *106*, 5151.
4. H. Zhang, L.-L. Wang, X.-Y. Pang, L.-P. Yang, W. Jiang, *Chem. Commun.*, **2021**, *57*, 13724-13727.
5 Clark, R. C.; Reid, J. S. *Acta Cryst.,* **1995**, *A51*, 887.
6 Sheldrick, G. M. *Acta Cryst.,* **2008**, *A64*, 112-122.